Ottensite, brizziite and mopungite from Pereta mine (Tuscany, Italy): New occurrences and crystal structure refinement of mopungite

Ottensite, brizziite and mopungite from Pereta mine (Tuscany, Italy): New occurrences and crystal structure refinement of mopungite

ERICA BITTARELLO[1,2*], FERNANDO CÁMARA[1,3], MARCO E. CIRIOTTI[2], ALESSANDRA MARENGO[1]

[1]Dipartimento di Scienze della Terra, Università degli Studi di Torino, via Tommaso Valperga Caluso 35, I-10125 Torino, Italy

[2]Associazione Micromineralogica Italiana, via San Pietro 55, I-10073 Devesi-Cirié, Torino, Italy

[3]CrisDi, Interdepartmental Centre for the Research and Development of Crystallography, via Pietro Giuria 7, I-10125, Torino, Italy

*E-mail: erica.bittarello@unito.it – tel +390116705130 – Fax +390116705128

ABSTRACT

Ottensite, $Na_3(Sb_2O_3)(SbS_3)\cdot 3H_2O$, brizziite, $NaSbO_3$, and mopungite, $NaSb(OH)_6$, have been found on several specimens from the antimony mine of Pereta (Grosseto, Tuscany, Italy).

Ottensite from Pereta mine occurs as brilliant reddish-brown spheroidal aggregates, with a diameter up to 0.2 mm, formed by radially oriented individuals. These aggregates are associated with well-shaped tabular and pseudocubic colourless crystals of mopungite and platy aggregates of brizziite. This is the second world occurrence of ottensite and brizziite. The mineral species were characterized by electron microprobe analysis, X-ray diffraction study and microRaman spectroscopy. Single-crystal X-ray diffraction data were collected on a twinned crystal of mopungite and the structure was for the first time refined on a natural sample in space group $P4_2/n$ [unit cell parameters a = 8.036(3) Å, c = 7.926(6) Å, V = 511.88(5) Å^3, Z = 4] obtaining an R_1-index of 5.17, wR_2 of 13.52 and GooF of 1.247.

Keywords: brizziite; mopungite; ottensite; crystal structure; Pereta mine; Tuscany; Italy

Introduction

In 2013, the mineral collectors Gabriele Zaccaria and Giampiero Piva provided us with some samples (collected about 25 years ago) from Pereta mine (Tuscany, Italy) (Fig. 1). Botryoidal and stalactitic red-brown brilliant aggregates in association with pseudocubic to lamellar crystals attracted our attention (Fig. 2). Further investigations showed the specimens to correspond to ottensite, $Na_3(Sb_2O_3)(SbS_3)\cdot 3H_2O$ (Sejkora and Hyršl 2007), brizziite, $NaSbO_3$ (Olmi and Sabelli 1994) and mopungite, $NaSb(OH)_6$ (Williams 1985).

The antimoniferous mine of Pereta (42°38'37"N; 11°21'28"E) is located about 5 km S-SE of Scansano (Grosseto province, Tuscany, Italy) bordering on the sulphur-cinnabar Zolfiere mine (Fig. 1). Relevant historical, geological and mineralogical researches have been conducted on Pereta mine. Geology and ore bodies were studied in detail by

Coquand (1848), Lotti (1901), Zaccagnini (1953), Dessau and De Stefanis (1969), Dessau (1971), Stea (1971), Sorelli (1985) and Brizzi and Meli (1995).

Contrary to what is documented for the nearby Zolfiere mine, there is no convincing information about a plausible exploitation of Pereta mine in the Etruscan and Roman ages. Mining activities in the 18th and 19th centuries are well-attested and, as reported, frequently interrupted because of carbon and sulphur dioxides exhalations.

Nowadays, the old Pereta mine is one of the most popular mineral collecting localities in Tuscany, and recent drill holes have brought to the surface some new and interesting material. Pereta is the type locality for two mineral species: peretaite, $CaSb^{3+}{}_4O_4(SO_4)_2(OH)_2{\cdot}2H_2O$ (Cipriani et al. 1980a) and coquandite, $Sb_6O_8(SO_4){\cdot}H_2O$ (Sabelli et al. 1992). Many other rare minerals have also been found and at present about 35 valid species have been identified at Pereta. Klebelsbergite, $Sb_4O_4(OH)_2SO_4$ (Zsivny 1929; Nakai and Appleman 1980) and mopungite found at Pereta mine were the second world finding (Cipriani et al. 1980b; Marzoni Fecia di Cossato et al. 1987, respectively). Minyulite, $KAl_2(PO_4)_2(OH,F){\cdot}4H_2O$ (Simpson and LeMesurier 1932) and fluellite, $Al_2(PO_4)F_2(OH){\cdot}7H_2O$ (Lévy 1824) were reported in Italy for the first time from Pereta mine (Menchetti and Sabelli 1981).

Ottensite, $Na_3(Sb_2O_3)(SbS_3){\cdot}3H_2O$, is the Na-dominant analogue of cetineite, $(K,Na)_{3+x}(Sb_2O_3)_3(SbS_3)(OH)_x{\cdot}2.4H_2O$ ($x \sim 0.5$) (Sabelli and Vezzalini 1987), and was discovered at Qinglong (Qinglong County, Guizhou Province, China; Sejkora and Hyršl 2007), where it was found as crusts, spheres and columnar aggregates on well-formed terminated stibnite crystals. The spheres typically had a smooth and lustrous surface, but in some cases were composed of crystals with a hexagonal prism {100}. Crystals were red-brown, brittle, with a vitreous lustre. The mineral was described as being a sodium oxo-antimoniate hydrate, with hexagonal symmetry, a = 14.1758(2) and c = 5.5712(1) Å, space group $P6_3$. Origlieri et al. (2007) reported on the paragenesis of known occurrences of ottensite.

Brizziite, $NaSbO_3$ (Olmi and Sabelli 1994), is a sodium antimonate that occurs as dense aggregates of platy {001} colourless and transparent, with pearly lustre hexagonal crystals. So far, it has been described from the Cetine mine (Siena province, Tuscany, Italy) and the associated minerals are stibiconite and mopungite. The unit cell is rhombohedral (hexagonal) a = 5.301(1), c = 15.932(4) Å, space group R-3 and Z = 6.

Mopungite is a member of the stottite group of perovskite-related hydroxides family with formula $NaSb(OH)_6$. It was first described by Williams (1985) from the Green Prospect in the Mopung Hills (Churchill County, Nevada, USA) where it occurs as encrustations of small pseudocubic colourless or milky-white crystals 0.2-0.3 mm on an edge. In that locality, the genesis of mopungite and other antimony basic oxides and sulphates is interpreted as due to the oxidation of stibnite crystals on the surface of the deposit.
Williams (1985) carried out a X-ray powder diffraction study on mopungite and showed that the mineral is tetragonal, space group $P4_2/n$ with lattice dimensions a = 7.994, c = 7.859 Å. The chemical composition, determined through energy-dispersive X-ray fluorescence, gave Na_2O 12.8, Sb_2O_5 65.2 and H_2O 22.0, recalculated to 100% after deduction of insoluble native sulphur 11.1% (Williams 1985). The empirical formula, normalized to 6 oxygen atoms, is $Na_{1.01}Sb_{0.99}(OH)_6$, i.e. ideally $NaSb(OH)_6$.

Although there is no particular scarcity of natural mopungite, difficulties were encountered in separating pure material for analysis by Williams (1985) who noted a close similarity in composition between natural and synthetic material. The synthetic compound has been known for a long time and was studied in the past (Terreil 1866; Cormimboeuf 1892; Beintema 1937; Schrewelius 1938 and references herein).

Schrewelius (1938) provided some crystallographic data on the synthetic analogous $NaSb(OH)_6$ (space group $P4_2/n$, a = 8.01, c = 7.88 Å, V = 505.6 Å^3). More recently, the crystal structure of synthetic sodium hexahydroxoantimonate(V), $NaSb(OH)_6$, was refined by Asai (1975) in space group $P4_2/n$, a = 8.029(2), c = 7.894(3) Å, V = 508.9 Å^3, Z = 4. So far, no crystal structure determination was done on the naturally occurring material.

Paragenesis, occurrence and related minerals

Ottensite found at Pereta mine shows the same morphologies as observed in the type locality of Qinglong (China) and it commonly grows directly on well-formed stibnite surfaces or within fractures. Like at Qinglong (Origlieri et al. 2007), also at Pereta, it is considered a supergene product of stibnite weathering in the oxidation zone and at the Pereta mine ottensite aggregates grow directly on stibnite crystals. They occur as spheroidal aggregates, in some cases overlapping and during the growth process coalescing to form botryoidal and stalactitic aggregates (Fig. 3a, b). Each sphere, with a diameter up to 0.2 mm (Fig. 3d), is formed by radially oriented-individuals (Fig. 3c) which are brilliant reddish-brown, but in some cases show light and dark orange tints.
The associated minerals found in the specimens studied from Pereta mine are: metastibnite, quartz, calcite, valentinite, brizziite and mopungite. All have been identified by quantitative chemical analysis and microRaman spectroscopy.

Mopungite, $NaSb(OH)_6$, grows as well-shaped tabular and pseudocubic (Fig. 4a) colourless and milky white crystals with maximal size of 0.05 × 0.06 mm (Fig. 4c). It is associated with spherulitic aggregates of ottensite (Fig. 4b, c) and flattened, sometimes elongated, colourless aggregates of brizziite (Fig. 4d). The largest crystals of brizziite have dimensions up to 0.05 × 0.02 mm.

EXPERIMENTAL METHODS

Chemical data

The chemical composition was determined using a Cambridge Stereoscan 360 Scanning Electron Microscope, equipped with an Oxford Inca Energy 200 EDS microanalysis, Pentafet detector and ultrathin window for the determination of elements with Z number down to boron. All the spectra were obtained at 15 kV accelerating voltage, 25 mm working distance and 1 µA probe current, exposure time comprised between 60 and 300 seconds. Primary standardization was performed on SPI Supplies and Polaron Equipment analytical standards, regularly standardized against the high purity metallic cobalt standard.

Ottensite botryoidal aggregates were embedded in epoxy resin to prepare a tablet, consequently polished and carbon coated for analysis. The studied crystals were found to be homogeneous. The average values of 16 analyses are given in Table 1. The atomic contents were recalculated assuming 15 anions *apfu* and normalization of analyses yield the following formula $(Na_{2.82}K_{0.07})_{\Sigma=2.89}(Sb_2O_3)_3(Sb_{0.90}S_{2.88})\cdot 3H_2O$ and the results are in good agreement with the composition of ottensite reported by Sejkora and Hyršl (2007).

Polished and carbon coated platy colourless aggregates of brizziite were also analysed. A total of 6 points analysis was collected and the analytical data are reported in Table 1. The results show homogeneous composition, with sodium, antimony and oxygen as major elements and negligible traces of sulphur (due to the contamination of ottensite and stibnite), arsenic and iron (not quantified). Assuming 3 oxygen *apfu*, normalization of analyses yield the following formula $Na_{1.07}Sb_{0.98}O_3$, in agreement with the composition of brizziite (Olmi and Sabelli 1994).

The semiquantitative results on Pereta mopungite crystals show the presence of Na, Sb and minor S (average values of 7 analyses are given in Table 1). During the analyses the mopungite crystals decompose. The low Na_2O values (and so the higher value for Sb_2O_5) are due to the volatilization of Na under the electron beam (Autefage and Conderc 1980) as also reported by Marzoni Fecia di Cossato et al. (1987) on Pereta mopungite. The Na loss was reduced by modifying the analytical setup decreasing the exposure time to 60 seconds. However, the observed formula on the basis of 6 oxygen *apfu* $Na_{0.95}Sb_{0.97}(OH)_6$ is in agreement with the chemical composition and the ideal formula of mopungite, $NaSb(OH)_6$ (Williams 1985; Marzoni Fecia di Cossato et al. 1987).

MicroRaman Spectroscopy

Raman spectra were obtained using a micro/macro Jobin Yvon Mod. LabRam HRVIS, equipped with a motorized *x-y* stage and an Olympus microscope. The backscattered Raman signal was collected with 50 × objective and the Raman spectrum was obtained for a non-oriented crystal. The 632.8 nm line of an He-Ne laser was used as excitation; laser power (20 mW) was dosed by means of a series of density filters. An aperture of 100 μm was used to reduce the beam dose. The lateral and depth resolution were about 2 and 5 μm, respectively. The system was calibrated using the 520.6 cm^{-1} Raman band of silicon before each experimental session. The spectra were collected with multiple and repeated acquisitions (2 to 6) with single counting times ranging between 20 and 180 seconds to improve the signal-to-noise ratio in the spectra. Spectral manipulation such as baseline adjustment, smoothing and normalization were performed using the Labspec 5 software package (Horiba Jobin Yvon GmbH 2004, 2005). Band component analysis was undertaken using a Lorentzian function (Fityk software package, Wojdyr 2010).The Raman spectra of ottensite, mopungite and brizziite from Pereta mine are shown in Figs. 5a, b and c, respectively.

X-ray diffraction

Powder diffraction

The X‑ray powder diffraction patterns have been carried out by spinning crystal aggregates or a single crystal using an Oxford Gemini R Ultra diffractometer equipped with a CCD area detector, with graphite-monochromatized Mo*K*α radiation (λ = 0.71073 Å). Data were integrated and corrected for Lorentz and polarization, background effects, and absorption, using the package CRYSALIS^{Pro} (Agilent 2011).

X-ray powder diffraction data on a spheroidal aggregate (diameter 0.02 mm) of ottensite were collected in transmission mode in the 6-76° 2θ angular range, using a Mo*K*α radiation (λ = 0.71073 Å); step width = 0.010°; exposure time of 150 sec; with a fixed crystal-to-detector distance of 55 mm; 50 kV/40 mA and no internal standard used. Standard phi scan circle movement was used to produce the orientational statistics required for the powder experiment. The strongest reflections in the pattern are [*d*(Å)(*I*)(hkl)]: 4.61(45)(120), 4.10(50)(201), 2.97(80)(221), 2.90(100)(131), 2.67(45)(410). The unit-cell parameters refined from the powder data with the software GSAS (Larson and Von Dreele 1994) were obtained using the intensity extraction method: Rietveld; profile fitting function: fundamental parameters and background modelling: shifted Chebychev polynomials). Lattice parameters are a = 14.112(6), c = 5.552(4) Å, and V = 963.5(6) Å^3 in agreement with those reported for the ottensite by Sejkora and Hyrsl (2007) and the X-ray powder pattern is very similar to that of cetineite (Sabelli and Vezzalini 1987).

Mopungite powder X–ray diffraction pattern was obtained from the single crystal experiment. Software CRYSALISPro (version 171.37.35, Agilent 2011) allows to use the images obtained from a single crystal in order to extract the powder pattern by collapsing 3D data, processing data frame by frame. The pattern was used to refine unit-cell parameter data starting from the mopungite structural model refined from single crystal data using the software GSAS (Larson and Von Dreele 1994), results are reported in Table 2. We obtained the following unit-cell parameters: a = 8.044(9), c = 7.91(10) Å, V = 511.8(9) Å^3, they are slightly larger than those reported by Asai (1975): a = 8.029(2), c = 7.894(3) Å, V = 508.9 Å^3. We were not able to separate brizziite crystals for a powder or single crystal X–ray diffraction study.

Single crystal X-ray diffraction

Diffraction intensity data were collected on a twinned crystal of mopungite (approximately 0.10 × 0.10 × 0.06 mm) on an Oxford Gemini R Ultra diffractometer equipped with a CCD area detector, with graphite-monochromatized Mo*K*α radiation (λ = 0.71073 Å). Crystallographic data and experimental conditions are summarized in Table 3. The intensities of 11364 reflections with $-10 < h < 11$, $-10 < k < 11$, $-10 < l < 10$ were collected to 58.48° 2θ using 0.2° frame and an integration time of 10 s. Data were integrated and corrected for Lorentz and polarization, background effects, and absorption, using the package CRYSALIS^{Pro} (Agilent 2011). Refinement of the unit-cell parameters was based on 11212 measured reflections with $I > 10\sigma(I)$. At room temperature, the unit-cell parameters are a = 8.036(3), c = 7.926(6) Å, V = 511.88(5) Å^3, space group $P4_2/n$, Z =4. The a:c ratio is 1:0.9863. A total of 675 independent reflections was collected.

The crystal structure of mopungite was refined using the SHELX set of programs (Sheldrick 2008), starting from the atom coordinates of stottite (Kleppe et al. 2012). The structure has the same topology as the one reported by Schrewelius (1938) and Asai (1975) on synthetic analogous of mopungite, $NaSb(OH)_6$, but differs in the choice of the origin of the space group. In accordance with the data on other members of the stottite group, we chose to use the structure coordinates setting of stottite as described by Ross et al. (1988) and Kleppe et al. (2012). Scattering curves for neutral atoms were taken from International Tables for Crystallography (Wilson 1992). Site-scattering values were refined at the first stages but converged to values close in the last refinement and therefore were fixed to full occupancy. Refinement converged to R_1 = 10.41%. We tested the model with routine TwinRotMat in PLATON (V-11010) (Spek 2009) that showed the presence of a merohedral twin consisting of a 180° rotation around [110]. We added the twin to the model, which converged to R_1 = 5.1% for 521 observed reflections with $F_o > 4\sigma(F_o)$ and 41

parameters. The refined twin proportion was 0.48(1). Tables 4, 5 and 6 report the atomic coordinates, displacement parameters and selected bond distances and angles, respectively.

Kleppe et al. (2012) supposed that the actual symmetry of stottite at ambient conditions is monoclinic $P2/n$ on the basis that their observed Raman spectrum for the (OH) stretching region was incompatible with the $P4_2/n$ symmetry, but their results from diffraction were not conclusive. Ross et al. (1988), who reported $P4_2/n$ symmetry, also discussed assignment of tetragonal symmetry to stottite. Again, their single crystal data did not fully justify assigning lower symmetry, but they observed that Strunz et al. (1958) reported a biaxial optical character for stottite. Synthetic hydroxide-perovskite $MgSi(OH)_6$, known as the ''3.65 Å-phase'' (Wunder et al. 2011), has pseudo-orthorhombic symmetry but the computational study of Wunder et al. (2012) indicates that the structure is very likely monoclinic $P2_1$. Welch and Wunder (2012) studied crystals of the high-pressure synthesis of Wunder et al. (2011) by single crystal diffraction and reported space group $P2_1/n$, which is a common space group for double perovskites. Following these authors, this symmetry would imply 3 OH-stretching peaks in the Raman spectrum, whereas spectroscopy sees ≥ 6 peaks (Wunder et al. 2011), and would imply $P2_1$ symmetry, at least at local level. We tested also the monoclinic $P2/n$ model of Kleppe et al. (2012) starting from their coordinates. Analysis of the model with isotropic displacement parameters showed high R-index due to the presence of twinning. TwinRotMat (Spek 2009) reported the significant presence of two twinning operations: a 180° rotation on [100] with composition plane on (100) and a 180° rotation around [10-1] with composition plane (10-1). Refinement of the model using a HKLF file generated with PLATON (Spek 2009) converged to low R-index (R_1 = 5.17%, Table 3) and the observed twin proportions, which refer to the contributions of the two minor twin components, were 0.17(2) and 0.35(2). Two oxygen atoms (O1 and O2) yielded non positive definite displacement parameters and were refined isotropically. Analysis with AddSym showed that the $P4_2/n$ symmetry was missing, therefore we kept the $P4_2/n$ model. CIF file of the monoclinic model is available as electronic supplemental material.

RESULTS

Ottensite

There is a close matching between the collected spectrum and that of ottensite from type locality of Qinglong County (China) in the RRUFF database (R070115; Downs 2006) (Fig. 5a). The spectrum for ottensite was acquired in the range 150-1200 cm^{-1} and Figure 5a shows the portion between 200 and 850 cm^{-1} for a better comparison with the relative RRUFF spectral range. The strongest Raman bands of ottensite from Pereta mine are at 153, 299, 344, 355 and 538 cm^{-1}. Other weaker, broad and multiple bands are visible at 225, 254, 479, 615 and 766 cm^{-1}.

Mopungite

The microRaman spectrum of mopungite crystals from Pereta mine is compared in Figure 5b with Raman spectrum of mopungite from Cetine mine (Siena Province, Tuscany, Italy) studied by Rintoul et al. (2010). These authors report band assignments according to symmetry and chemical composition. There is no Raman information in the RRUFF on-line database (Downs 2006). Before the work of Rintoul et al. (2010) synthetic equivalent samples of mopungite had been studied by infrared spectroscopy (Balicheva and Roi 1971; Franck 1973). The spectrum for mopungite from Pereta mine was recorded in the range 150-4000 cm^{-1}. In the region between 200 and 400 cm^{-1}, the

spectrum shows the two most intense bands at about 350 and 362 cm^{-1} (compared to 349 and 361 cm^{-1}; Rintoul et al. 2010) that correspond to γ(OH), Sb-O deformations or δ(Sb-O), while bands lower than 200 cm^{-1} correspond to lattice modes (189 and 204 cm^{-1}, compared to 188 and 204 cm^{1}; Rintoul et al. 2010). In the region of 400-800 cm^{-1} the spectrum shows complexity with multiple bands and shoulders observed and these bands can be attributed to Sb-O stretching. A more intense broad envelope of overlapping bands centred around 626 cm^{-1} (to be compared to 625 cm^{-1} reported by Rintoul et al. 2010). Peak-fitting allows bands to be resolved in components at 605, 648, 671 cm^{-1} (to be compared to 604, 649 and 669 cm^{-1} reported by Rintoul et al. 2010).

In the range 2800-3600 cm^{-1} the spectrum is complex showing multiple bands (Fig. 6). Peak fitting of the broad overlapping bands reveals that there are three components present at 3134, 3178 and 3239 cm^{-1} (compared to 3176, 3184 and 3235 cm^{-1}; Rintoul et al. 2010). A broad weaker band centred at 3342 cm^{-1} may be resolved into two component bands at 3331 and 3353 cm^{-1} (to be compared to 3315 cm^{-1} reported by Rintoul et al. 2010). A more intense sharp band occurs at 3423 cm^{-1} (matching 3423 cm^{-1} peak by Rintoul et al. 2010). Kleppe et al. (2012) observed also 6 bands in the range 2800-3600 cm^{-1} of their Raman spectrum of stottite and they interpreted this fact as an implication of monoclinic instead of tetragonal symmetry in stottite, based on the fact that the number of symmetrically independent oxygen atoms is doubled in the monoclinic model ($P2/n$). Also, the synthetic high-pressure hydroxide perovskite $MgSi(OH)_6$ is metrically pseudo-orthorhombic but refines as structurally monoclinic with $P2_1/n$ (Welch and Wunder, 2012), but Raman spectroscopy shows six OH-stretching peaks (not three expected for $P2_1/n$) which implies lower symmetry ($P2_1$). In absence of a detailed analysis of symmetry degeneracies of vibrational modes due to the reduction of symmetry and considering our diffraction data inconclusive, we are not prone to conclude the lowering of symmetry for natural mopungite, at least a room-conditions.

Brizziite

Raman spectrum on brizziite aggregates is shown in Fig. ~~ure~~ 5c where it is compared to that of brizziite from the type locality of Cetine mine (Siena province, Tuscany, Italy) available in the RRUFF database (R060611) (Downs 2006). There is accordance between the positions of the bands of both Raman spectra, but the slight discrepancy of the intensity of some peaks is due to the crystal orientation effect. The spectrum for brizziite was acquired in the range 120-1200 cm^{-1} and Fig. ~~ure~~ 5c shows the portion between 120 and 1000 cm^{-1} for a better comparison with the relative RRUFF spectral range. The strongest bands of brizziite from Pereta mine are at 157, 202, 225, 301, 335, 490, 629 and 658 cm^{-1}, in agreement with observations on brizziite from Cetine mine (Frost and Bahfenne 2010). The strongest Raman bands at 658 and 629 cm^{-1} are attributed to the SbO_3^- symmetric stretching mode following Frost and Bahfenne (2010). Broad band at 490 cm^{-1} is ascribed to SbO antisymmetric stretching vibrations, and the weaker and multiple bands visible at 202, 225, 301 and 335 cm^{-1} are assigned to O-Sb-O bending modes (Frost and Bahfenne 2010).

Structure topology of mopungite and related minerals

Mopungite is an heterovalent hydroxide-perovskite compound with an empty *A*-site. It is the Na–Sb analogue of stottite, $FeGe(OH)_6$ (Strunz et al. 1958; Strunz and Giglio 1961; Ross et al. 1988) and the only known Sb member of the stottite group. Furthermore, mopungite is the only antimonate hydroxide-perovskite known so far. The structure has two symmetrically distinct *B*-sites which are coordinated by corner-sharing oxygen octahedra with alternating sense of rotation in three dimensions. The heterovalent cations (Na^+ and Sb^{5+}) alternate along the crystal axes due to

bond-valence constraints avoiding over-bonding at the oxygen sites (Kleppe et al. 2012). The structure type can show distortion leading to either cubic or tetragonal symmetries. Recently, Kleppe and co-workers (2012) discussed the possibility of the monoclinic symmetry in stottite in which the two distinct B-sites are divided in two pairs of symmetrically independent sites.

The space groups and lattice parameters of heterovalent hydroxide-perovskites are compared in Table 7.

In the mopungite structure (Figs. 7-8) the antimony atom is surrounded by six oxygen atoms, so the polyhedron is a nearly regular octahedron with mean interatomic distances of 1.976 Å for Sb−O and 2.792 Å for O−O (in agreement with 1.98 Å for Sb–O and 2.80 Å for O–O; Asai 1975). The coordination polyhedron of sodium is a nearly regular octahedron, with mean interatomic distances of 2.404 Å for Na−O and 3.399 Å for O−O (compared to 2.39 Å for Na–O and 3.38 Å for O–O; Asai 1975). Observed distances are in agreement with predicted ionic radii from Shannon (1976), i.e. 1.96 Å for Sb−O and 2.38 Å for Na−O. The tentative refinement of a monoclinic *P*2/*n* model yielded two slightly different *Sb*-sites, one slightly larger than the other: <Sb1−O> = 1.972(9) Å and <Sb2−O> = 1.981(9) Å, but equal within errors. The same thing was observed for the Na sites: <Na1−O> = 2.397(9) Å and <Na2−O> = 2.412(9) Å. Considering that we have very weak data on the (OH) stretching region (see Raman) and therefore we had no strong argument for monoclinic symmetry, as we said above, we opt to keep the tetragonal model.

In $P4_2/n$ stottite structure both the Fe and Ge coordination polyhedra are nearly regular octahedra, but the Fe–O–Ge angles average about 136.3° (Ross et al. 1988) and 137.1° (Kleppe et al. 2012), indicating that most of the distortion from isometric symmetry in the structure is taken up by rigid rotation of the polyhedra. In mopungite Na and Sb coordination octahedra also remain relatively regular, but the Na–O–Sb angles average about 131.6°, while it is 135.1° in burtite and 137.5° in schoenfliesite (Basciano et al. 1998). This implies a lager rotation of octahedra in mopungite.

Basciano et al. (1998) gave evidence, through neutron powder diffraction, that in burtite and schoenfliesite the locations of H atoms are disordered. The quality of our data did not allow the location of hydrogen atoms.

Acknowledgements

FC and EB thank Ministero dell'Istruzione, dell'Università e della Ricerca and Associazione Micromineralogica Italiana for the co-funding of a research contract for EB for the year 2013.

References

Agilent (2011) CrysAlis PRO. Agilent Technologies Ltd, Yarnton, England

Asai T (1975) Refinement of the cCrystal sStructure of sSodium hHexahydroxoantimonate(V), $NaSb(OH)_6$. B Chem Soc Jpn 48(10):2677-2679

Autefage F, Conderc JJ (1980) Étude du mécanisme de la migration du sodium et du potassium au cours de leur analyse à la microsonde électronique. Bull Mineral 103:623-629

Balicheva TG, Roi NI (1971) IR spectra and structure of several crystalline hexahydroxyantimonates and their deutero analogs. J Struct Chem 12(3):384-390

Basciano LC, Peterson RC, Roeder PL, Swainson I (1998) Description of schoenfliesite, $MgSn(OH)_6$, and roxbyite, $Cu_{1.72}S$, from a 1375 BC shipwreck, and Rietveld neutron-diffraction refinement of synthetic schoenfliesite, wickmanite, $MnSn(OH)_6$, and burtite, $CaSn(OH)_6$. Can Mineral 36:1203-1210

Beintema, J (1937) Die Struktur einiger kKristallisierternn Antimonate. Recl Trav Chim Pays-Bas 56(10):931-967

Betterton J, Green DI, Jewson C, Spratt J, Tandy P (1998) The composition and structure of jeanbandyite and natanite. Mineral Mag 62:707-712

Brizzi G, Meli R (1995) La miniera antimonifera di Pereta con un cenno a quella solfo-cinabrifera di Zolfiere in comune di Scansano (GR). Riv Mineral Ita 19:217-240

Cipriani N, Menchetti S, Orlandi P, Sabelli C (1980a) Peretaite, a new mineral from Pereta, Tuscany, Italy. Am Mineral 65:936-936

Cipriani N, Menchetti S, Sabelli C (1980b) Klebelsbergite and another antimony mineral from Pereta, Tuscany, Italy. Neues Jb Miner Monatshefte 223-229

Cormimboeuf H (1892) Action de la potasse et de la soude sur l'oxyde d'antimoine. C R Acad Sci Paris 115:1305-1307

Coquand H (1848) Sur un filon antimonifère, les sulfates, les alunières et les lagoni de la Toscane, et sut l'accroissement de température en profondeur. Bull Soc Geol Fr, 2eme série, 6:91-160

Dessau G, De Stefanis A (1969) Studio geologico minerario della zona mercurifera di Cerreto Piano. Mem Soc Geol Ita 7:289-323

Dessau G (1971) I giacimenti dell'area di Scansano (Grosseto). Rend Soc Ital Mineral Petrol, "La Toscana Meridionale" 27: 489-501

Downs RT (2006) The RRUFF Project: an integrated study of the chemistry, crystallography, Raman and infrared spectroscopy of minerals. Program and Abstracts of the 19th General Meeting of the International Mineralogical Association in Kobe, Japan. O03-13

Faust GT, Schaller WT (1971) Schoenfliesite, $MgSn(OH)_6$. Z Kristallogr 134:116-141

Fedorov S (2008) GetData Graph Digitizer 2.26. http://getdata-graph-digitizer.com/ Moscow, Russia, 2008

Franck R (1973) Spectres d'absorption infrarouge de quelques hydroxyantimoniates. Rev Chim Miner 10:795-810

Frost RL, Bahfenne S (2010) Raman spectroscopic study of the antimonate mineral brizziite $NaSbO_3$. Radiat Eff Defect S 165(3):206-210

Horiba Jobin Yvon GmbH (2004, 2005) LabSpec [Software for Raman spectroscopic data analysis, 463 acquisition and manipulation]. Version 5.64.15

Kampf AR (1982) Jeanbandyite a new member of the stottite group from Llallagua, Bolivia. Mineral Rec 13:235-239

Kleppe AK, Welch MD, Crichton WA, Jephcoat AP (2012) Phase transitions in hydroxide perovskites: a Raman spectroscopic study of stottite, $FeGe(OH)_6$, to 21 Gpa. Mineral Mag 76:949-962

Larson AC, Von Dreele RB (1994) General sStructure sAnalysis sSystem (GSAS). Los Alamos National Laboratory Report (LAUR, 86-748), Los Alamos, New Mexico, pp 224

Lévy A (1824) On a new mineral substance. Ann Phylos 8:241-245

Lotti B (1901) I giacimenti cinabriferi ed antimoniferi della Toscana e la loro relazione con le rocce eruttive quaternarie. Rass Min 7:117-119 and 136-138

Marshukova NK, Palovskii AB, Sidorenko GA, Chistyakova NI (1981) Vismirnovite, $ZnSn(OH)_6$, and natanite, $FeSn(OH)_6$, new tin minerals. Zap Vses Mineral Obshchestva 110(4):492-500

Marshukova NK, Pavlovskii AB, Sidorenko GA (1984) Mushistonite, $(Cu,Zn,Fe)Sn(OH)_6$, a new tin mineral. Zap Vses Mineral Obshchestva 113(5):612-617

Marzoni Fecia di Cossato Y, Meacci C, Orlandi P, Vezzalini G (1987) The second world occurrence of mopungite from Pereta Mine, Tuscany, Italy. Atti Soc Toscana Sci Nat, Mem 94:135-138

Menchetti S, Sabelli C (1981) Minyulite, associated with fluellite, from Pereta, Tuscany, Italy. Neues Jb Miner Monat 11:505-510

Momma K, Izumi F (2011) VESTA 3 for three-dimensional visualization of crystal, volumetric and morphology data. J Appl Crystallogr 44:1272-1276

Moore PB, Smith JV (1967) Wickmanite, $Mn^{+2}[Sn^{+4}(OH)_6]$, a new mineral from Långban. Ark Mineral Geol 4:395-399

Morgenstern-Badarau I (1976) Effet Jahn-Teller et structure cristalline de l'hydroxyde $CuSn(OH)_6$. J Solid State Chem 17 (4):399-406

Morgenstern-Badarau I, Michel A (1976) Sur l'existence d'un oxyhydroxyde double de fer(III) et d'étain(IV). J Inorg Nucl Chem 38:1400-1402

Nakai I, Appleman DE (1980) Klebelsbergite, $SbO_4(OH)_2SO_4$: redefinition and synthesis. Am Mineral 65:499-505

Olmi F, Sabelli C (1994) Brizziite, $NaSbO_3$, a new mineral from the Cetine mine (Tuscany, Italy): description and crystal structure. Eur J Mineral 6:667-672

Origlieri MJ, Laetsch TA, Downs RT (2007) A note on the paragenesis of ottensite. Mineral Rec 38:83-84

Rintoul L, Bahfenne S, Frost RL (2010) Single-crystal Raman spectroscopy of brandholzite $Mg[Sb(OH)_6]_2 \cdot 6H_2O$ and bottinoite $Ni[Sb(OH)_6]_2 \cdot 6H_2O$ and the polycrystalline Raman spectrum of mopungite $Na[Sb(OH)_6]$. J Raman Spectrosc 42:1147-1153

Ross CR, Bernstein LR, Waychunas GA (1988) Crystal-structure refinement of stottite, $FeGe(OH)_6$. Am. Mineral 73:657-661

Sabelli C, Vezzalini G (1987) Cetineite, a new antimony oxide-sulfide mineral from Cetine mine, Tuscany, Italy. Neues Jb Miner Monat 419-425

Sabelli C, Orlandi P, Vezzalini G (1992) Coquandite a new mineral from Pereta, Tuscany, Italy, and two other localities. Mineral Mag 56:599-603

Schrewelius N (1938) Röntgenuntersuchung der V~~v~~erbindungen $NaSb(OH)_6$, $NaSb_6$, $NaSbO_3$ und gleichartiger S~~s~~toffe. Z Anorg Allg Chem 238:241-254

Sheldrick, GM (2008) A short history of SHELX. Acta Crystallogr A64:112-122

Sejkora J, Hyršl J (2007) Ottensite a new mineral from QingLong, Guizhou Province, China. Mineral Rec 38:77-81

Shannon RD (1976) Revised effective ionic radii and systematic studies of interatomic distances in halides and chalcogenides. Acta Crystallogr 32:751-767

Simpson ES, LeMesurier CR (1932) Minyulite, a new phosphate mineral from Dandaragan, W.A. J Royal Soc ~~-~~West Aust 19:13-16

Sonnet PM (1981) Burtite, calcium hexahydroxostannate, a new mineral from El Hamman, Central Morocco. Can Mineral 19:397-401

Sorelli M (1985) Una miniera maremmana dell'età preindustriale. Le zolfiere granducali di Pereta, dagli inizi all'abbandono della attività estrattiva (secoli XVIII-XIX). Bollettino della Società Storica Maremmana 49 in: http:/www.comune.scansano.gr.it/files/toponimi/sorelli.doc

Spek AL (2009) Structure validation in chemical crystallography. Acta Crystallogr D 65:148-155

Stea B (1971) Mineralizzazioni ad antimonio della Toscana meridionale: Zolfiere o Pereta (Scansano - Grosseto). Rend Soc Ital Mineral Petrol, Fascicolo Speciale "La Toscana Meridionale" 27:435-437

Strunz H, Söhnge G, Geier BH (1958) Stottit, ein Neues Germanium -Mineral, und seine Paragenese in Tsumeb. Neues Jb Miner Monat 85-96

Strunz VH, Giglio M (1961) - Die Kristallstruktur von Stottit $Fe[Ge(OH)_6]$. Acta Crystallogr 14:205-208

Terreil, A (1866) Des oxydes d'antimoine cristallisés et des antimonites. Ann Chim Phys 4(7):350-358

Welch MD, Wunder B (2012) A single-crystal X-ray diffraction study of the 3.65Å-phase $MgSi(OH)_6$, a high-pressure hydroxide-perovskite. Phys Chem Minerals 39: 693-697

White JS, Nelen JA (1973) Tetrawickmanite, tetragonal $MnSn(OH)_6$ a new mineral from North Carolina, and the stottite group. Mineral Rec 4:24-30

Williams SA (1985) Mopungite a new mineral from Nevada. Mineral Rec 16:73-74

Wilson AJC (1992) International Tables for Crystallography. Volume C: Mathematical, physical and chemical tables. Kluwer Academic Publishers, Dordrecht, The Netherlands

Wojdyr M (2010) Fityk: a general-purpose peak fitting program. J Appl Crystallogr 43:1126-1128

Wunder B, Wirth R, Koch-Müller M (2011) The 3.65 Å phase in the system MgO-SiO_2-H_2O: synthesis, composition, and structure. Am Mineral 96:1207-1214

Wunder B, Jahn S, Koch-Müller M, Speziale S (2012) The 3.65 Å phase, $MgSi(OH)_6$: structural insights from DFT calculations and T-dependent IR spectroscopy. Am Mineral 97:1043-1048

Zaccagnini C (1953) L'antimonio. L'Industria Mineraria 4:1-17

Zsivny V (1929) Klebelsbergit, ein neues Mineral von Felsöbánya. Matem és Természettudományi Értesitö 46:19-24

TABLE CAPTIONS

Table 1 Chemical composition of ottensite, brizziite and mopungite from Pereta mine. Values are based on the average of 16 analytical points for ottensite, 6 analytical points for brizziite, 7 analytical points for mopungite

Table 2 X–ray powder diffraction data for mopungite from Pereta mine. Simulated powder pattern obtained by collapsing single crystal diffraction frames acquired using an Oxford Gemini R Ultra diffractometer equipped with a CCD area detector, with graphite-monochromatized MoKα radiation. Refined unit-cell parameters: a = 8.036(3), c = 7.926(6) Å, V = 511.88(5) $Å^3$. Lp-correction = 0.5

Table3 Crystal data and summary of parameters describing data collection and refinement of the crystal structure of mopungite from Pereta mine

Table 4 Atomic parameters in the crystal structure of mopungite from Pereta mine. All atoms refined with full occupancy

Table 5 Anisotropic displacement parameters for atoms in the crystal structure of mopungite from Pereta mine

Table 6 Main interatomic distances (Å) and bond angles in the crystal structure of mopungite from Pereta mine

Table 7 Comparison of the symmetry and the crystal lattice parameters of heterovalent hydroxide-perovskites of general formula $BB'(OH)_6$. References are given in brackets

Table 1

	Ottensite		Brizziite		Mopungite		Standard
	Wt %	**Range**	**Wt %**	**Range**	**Wt %**	**Range**	
Na_2O	7.25	6.07-7.67	16.02	15.30-16.81	12.47	12.02-12.51	albite
S	7.66	7.14-8.19	-	-	-	-	anhydrite
K_2O	0.24	0-0.46	-	-	-	-	sanidine
Sb_2O_3	83.50	82.86-84.41	-	-	-	-	Sb
Sb_2O_5	-	-	79.40	76.38-82.79	66.59	65.48-67.85	Sb
Total	98.65		95.42		79.06		

Table 1 Chemical composition of ottensite, brizziite and mopungite from Pereta mine. Values are based on the average of 16 analytical points for ottensite, 6 analytical points for brizziite, 7 analytical points for mopungite

Table 2

h	k	l	d_{obs} (Å)	d_{calc} (Å)	I_{rel}	I_{calc}
1	1	1	4.618	4.618	100.00	100.0
0	2	0	4.022	4.018	68.92	67.4
0	0	2	3.956	3.963	55.58	26.7
2	2	0	2.844	2.841	11.77	7.6
0	2	2	2.820	2.822	58.88	21.4
1	3	0	2.544	2.541	7.95	1.2
0	3	1	2.539	2.538	6.83	4.3
1	1	3	2.422	2.396	17.85	12.6
2	2	2	2.309	2.309	12.40	10.9
0	4	0	2.011	2.009	33.47	10.4
3	3	1	1.831	1.831	5.86	5.5
2	4	0	1.799	1.797	6.17	12.7
0	4	2	1.793	1.792	28.33	19.1
0	2	4	1.775	1.777	9.14	17.7
2	4	2	1.637	1.637	14.01	19.0
2	2	4	1.624	1.625	25.01	16.4
3	3	3	1.539	1.539	10.60	3.6

Notes: *Only reflections with $I_{rel} > 6\sigma(I_{rel})$ are listed

Table 2 X–ray powder diffraction data for mopungite from Pereta mine. Observed powder pattern was obtained with using an Oxford Gemini R Ultra diffractometer equipped with a CCD area detector, with graphite-monochromatized MoKα radiation. Calculated pattern and indexing based on the refined unit-cell parameters: a = 8.036(3), c = 7.926(6) Å, V = 511.88(5) Å^3

Table 3

Crystal system	Tetragonal
Space group	$P4_2/n$
Unit–cell dimensions	
a (Å)	8.036(3)
c (Å)	7.926(6)
V (Å^3)	511.88(5)
Z	4
μ (mm^{-1})	5.42
F(000)	456
D_{calc} (g cm^{-3})	3.18
Crystal size (mm)	0.130 × 0.085 × 0.080
Radiation type	Mo $K\alpha$ (0.71073 Å)
Temperature (K)	293
2θ–range for data collection (º)	3.6-29.2
R_{int} (%)	8.43
Reflections collected	11364
Independent reflections	675
F_o>4σ(F)	518
Refinement method	least-squares matrix: full
No. of refined parameters	41
Final R_{obs} (%) all data	7.01
R_1 (%) F_o>4σ(F)	5.17
wR_2 (%) F_o>4σ(F)	13.52
Highest peak/deepest hole (e$^-$ Å^{-3})	1.143 / -0.84
Goodness of fit on F^2	1.247

Table 3 Crystal data and summary of parameters describing data collection and refinement of the crystal structure of mopungite from Pereta mine

Table 4

	Wyck.	*x*/*a*	*y*/*b*	*z*/*c*	U_{iso}
Na	4*c*	½	0	½	0.0199 (10)
Sb	4*d*	½	0	0	0.0160 (3)
O(1)	8*g*	0.2194 (8)	−0.0825 (8)	0.5730 (8)	0.0185 (13)
O(2)	8*g*	0.4453 (8)	0.2782 (8)	0.5959 (7)	0.0196 (13)
O(3)	8*g*	0.5679 (8)	−0.0897 (8)	0.7792 (7)	0.0177 (12)

*The temperature factor has the form exp(-T) where $T = 8\pi^2 U(\sin(\theta)/\lambda)^2$

Table 4 Atomic parameters in the crystal structure of mopungite from Pereta mine. All atoms refined with full occupancy*

Table 5

	U_{11}	U_{22}	U_{33}	U_{12}	U_{13}	U_{23}
Na	0.019 (3)	0.018 (3)	0.023 (3)	−0.0027 (18)	−0.003 (2)	0.000 (2)
Sb	0.0125 (5)	0.0159 (5)	0.0197 (5)	0.0003 (3)	0.0006 (3)	0.0011 (3)
O(1)	0.017 (3)	0.015 (3)	0.023 (3)	0.008 (3)	0.000 (3)	−0.008 (3)
O(2)	0.027 (3)	0.017 (3)	0.015 (3)	0.000 (3)	0.003 (3)	−0.003 (3)
O(3)	0.019 (3)	0.016 (3)	0.018 (3)	−0.005 (3)	0.000 (3)	−0.004 (3)

* The temperature factor has the form exp(-T) where $T = 2\pi^2\Sigma_{ij}(h(i)h(j)U(i,j)a^*(i)a^*(j))$

Table 5 Anisotropic displacement parameters for atoms in the crystal structure of mopungite from Pereta mine ($Å^2$)*

Table 7

	Formula	Space group	*a* (Å)	*b* (Å)	*c* (Å)	References
Stottite	$Fe^{2+}Ge^{4+}(OH)_6$	$P4_2/n$ $P2/n$	7.594 7.550	7.594 7.470	7.488 7.553	1, 2, 3
Mopungite	$NaSb^{5+}(OH)_6$	$P4_2/n$	8.0341	8.0341	7.9224	4
Jeanbandyite	$Fe^{3+}Sn^{4+}(OH,O)_6$	$P4_2/n$ $Pn3$	7.648 7.757	7.648 7.757	7.648 7.757	5,6 7
Tetrawickmanite	$Mn^{2+}Sn^{4+}(OH)_6$	$P4_2/n$	7.787	7.787	7.797	8
Mushistonite	$Cu^{2+}Sn^{4+}(OH)_6$	$Pn\bar{3}m$, $P4_2/nnm$	7.735 7.586	7.735 7.586	7.735 8.103	9 10
Burtite	$CaSn^{4+}(OH)_6$	$Pn3m$	8.128	8.128	8.128	11, 12
Natanite	$Fe^{2+}Sn^{4+}(OH)_6$	$Pn\bar{3}m$	7.722	7.722	7.722	13
Schoenfliesite	$MgSn^{4+}(OH)_6$	$Pn\bar{3}$	7.759	7.759	7.759	14, 12
Vismirnovite	$ZnSn^{4+}(OH)_6$	$Pn\bar{3}m$	7.80	7.80	7.80	13
Wickmanite	$Mn^{2+}Sn^{4+}(OH)_6$	$Pn\bar{3}$	7.873	7.873	7.873	15

(1) Strunz and Giglio 1961; (2) Ross et al. 1988; (3) Kleppe et al. 2012; (4) Williams 1985; (5) Kampf, 1982; (6) Betterton et al. 1998; (7) Morgenstern-Badarau and Michel 1976; (8) White and Nelen 1973; (9) Marshukova et al. 1984; (10) Morgenstern-Badarau 1976; (11) Sonnet 1981; (12) Basciano et al. 1998; (13) Marshukova et al. 1981; (14) Faust and Schaller 1971; (15) Moore and Smith 1967

Table 7 Comparison of the symmetry and the crystal lattice parameters of heterovalent hydroxide-perovskites of general formula $BB'(OH)_6$. References are given in brackets

FIGURE CAPTIONS

Fig. 1 Location of Pereta mine (Grosseto province, Tuscany, Italy)

Fig. 2 Photo and microscope images of the details of the sample analysed

Fig. 3 SEM images of botryoidal-stalactitic (a, b) and spherulitic (c, d) aggregates of ottensite from Pereta mine

Fig. 4 SEM images of pseudocubic aggregates of mopungite (a) that sometimes grow on spherulitic ottensite aggregates or in close association with them (b, c). Randomly oriented platy crystals of brizziite and pseudocubic crystals of mopungite (d) from Pereta mine

Fig. 5 Raman spectra of: a) spherulitic aggregates of ottensite compared to that of ottensite from type locality in the RRUFF database (R070115) (Downs 2006). b) pseudocubic crystals of mopungite compared to that of mopungite from Cetine mine (Siena, Italy) studied by Rintoul et al. (2010) (it was obtained by digitizing the original figure using GetData Graph Digitizer 2.26; Fedorov 2008). c) brizziite aggregates compared to that of brizziite from type locality of Cetine mine (Siena province, Tuscany, Italy) in the RRUFF database (R060611) (Downs 2006)

Fig. 6 Band-fitted spectrum of mopungite from Pereta mine in the 2800-3600 cm^{-1} region

Fig. 7 Arrangement of cation coordination polyhedra in mopungite (*c*-axis projection). Sb polyhedra are violet; Na are yellow. Graph obtained with VESTA v. 31.17. (Momma and Izumi 2011)

Fig. 8 Ball-and-stick model of a group of four coordination polyhedra from the structure of mopungite indicating the atom sites (*c*-axis projection). Graph obtained with VESTA v. 31.17. (Momma and Izumi 2011)

fig.1
Click here to download high resolution image

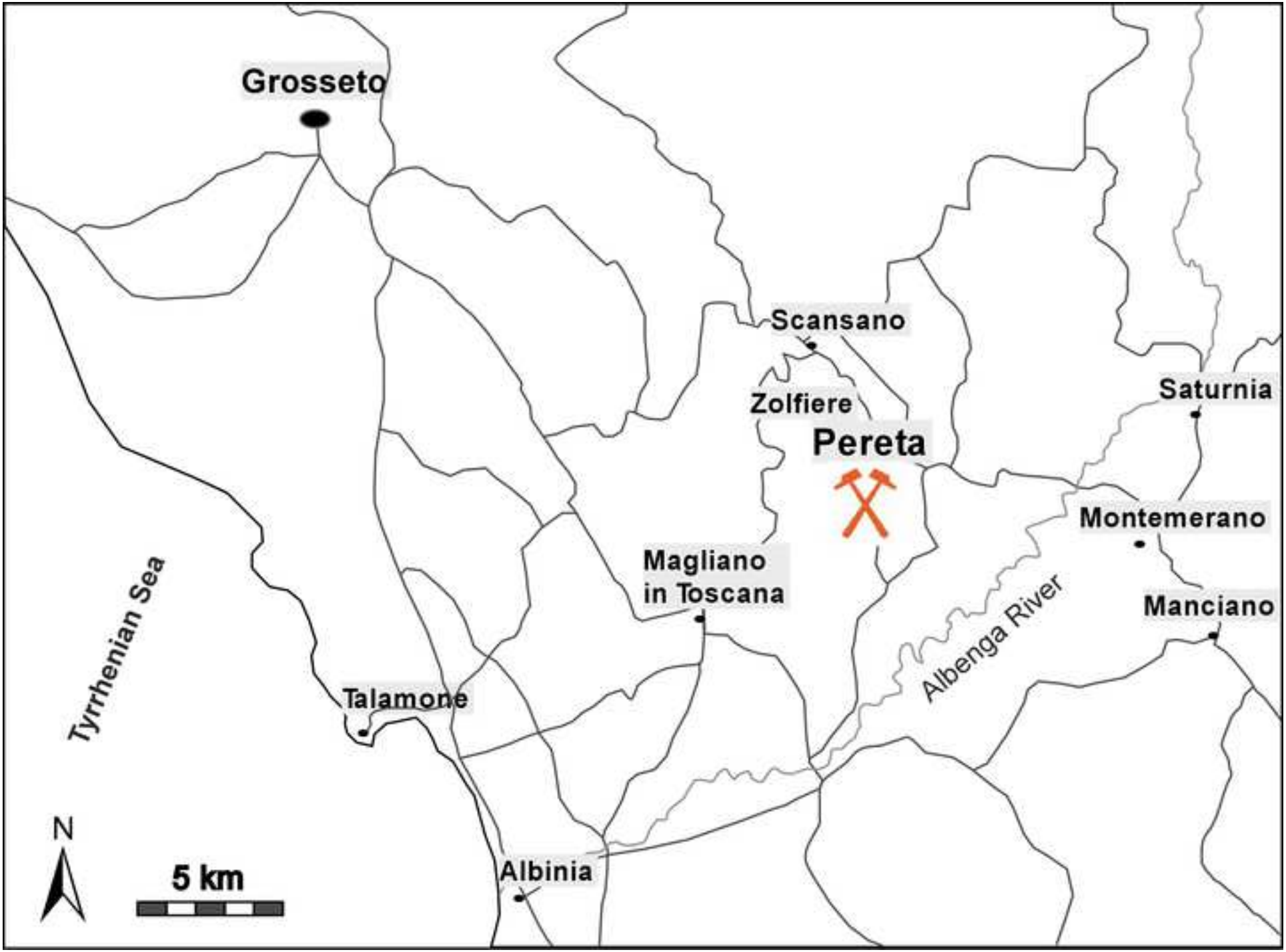

fig.2
Click here to download high resolution image

fig.3a
Click here to download high resolution image

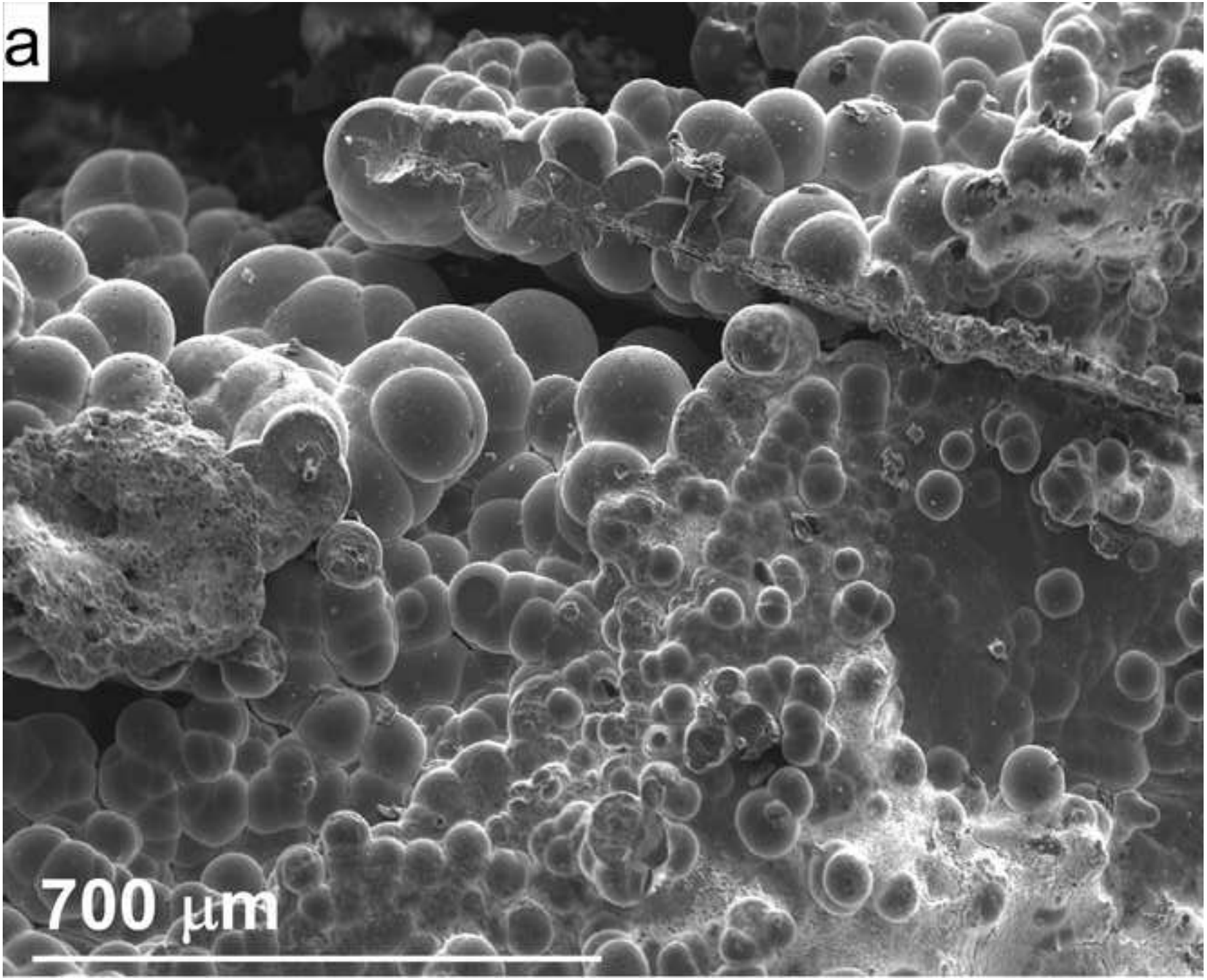

fig.3b
Click here to download high resolution image

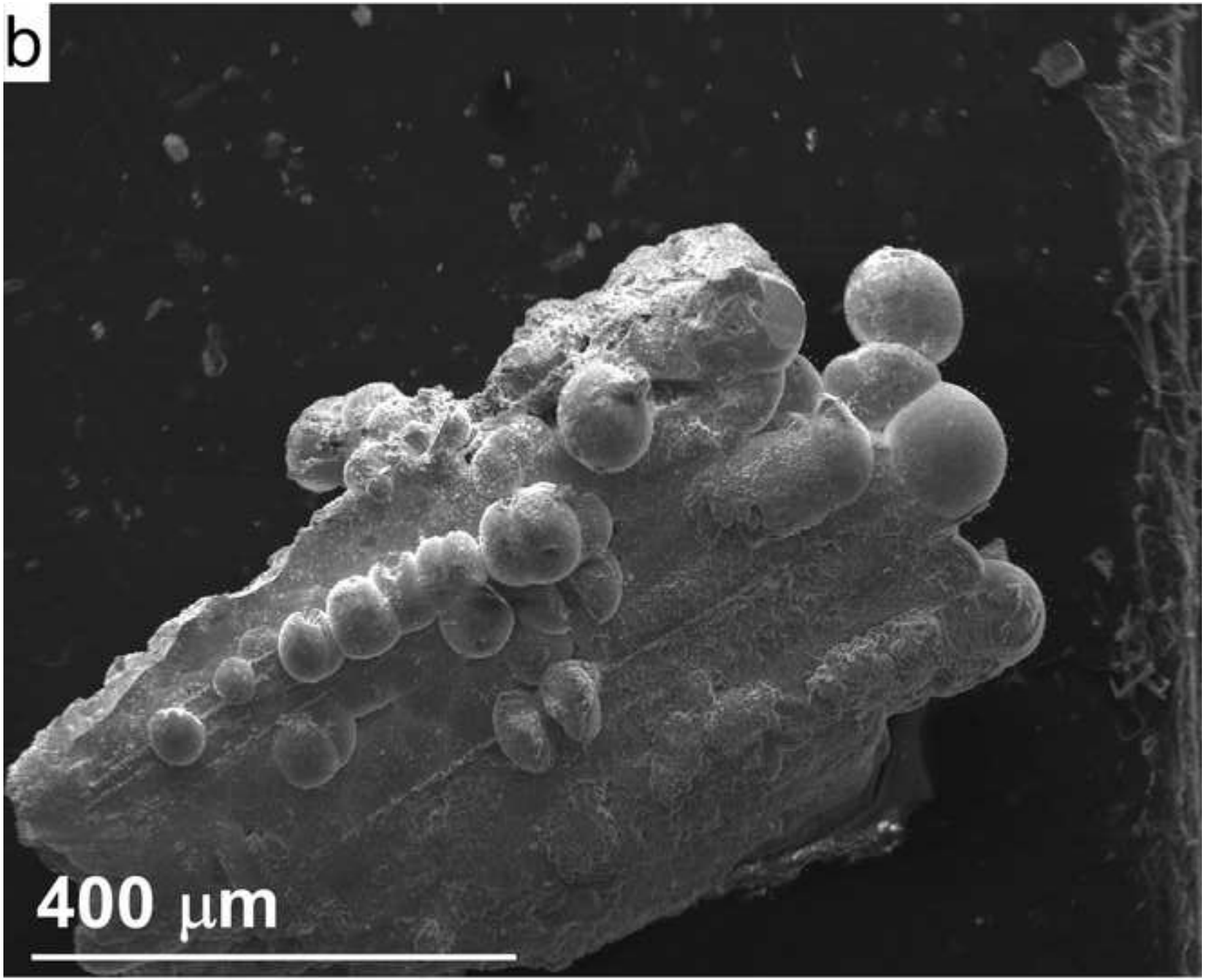

fig.3c
Click here to download high resolution image

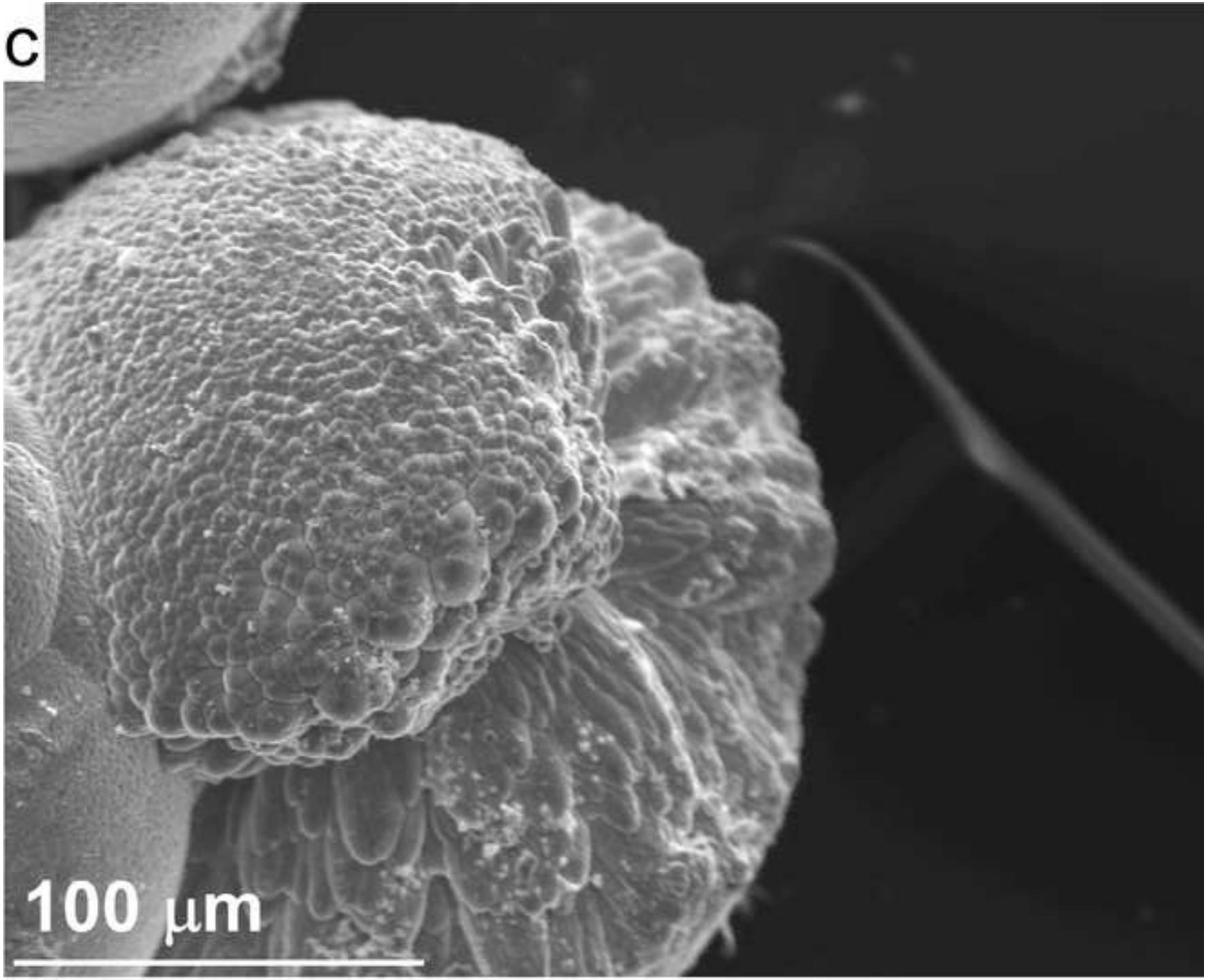

fig.3d
Click here to download high resolution image

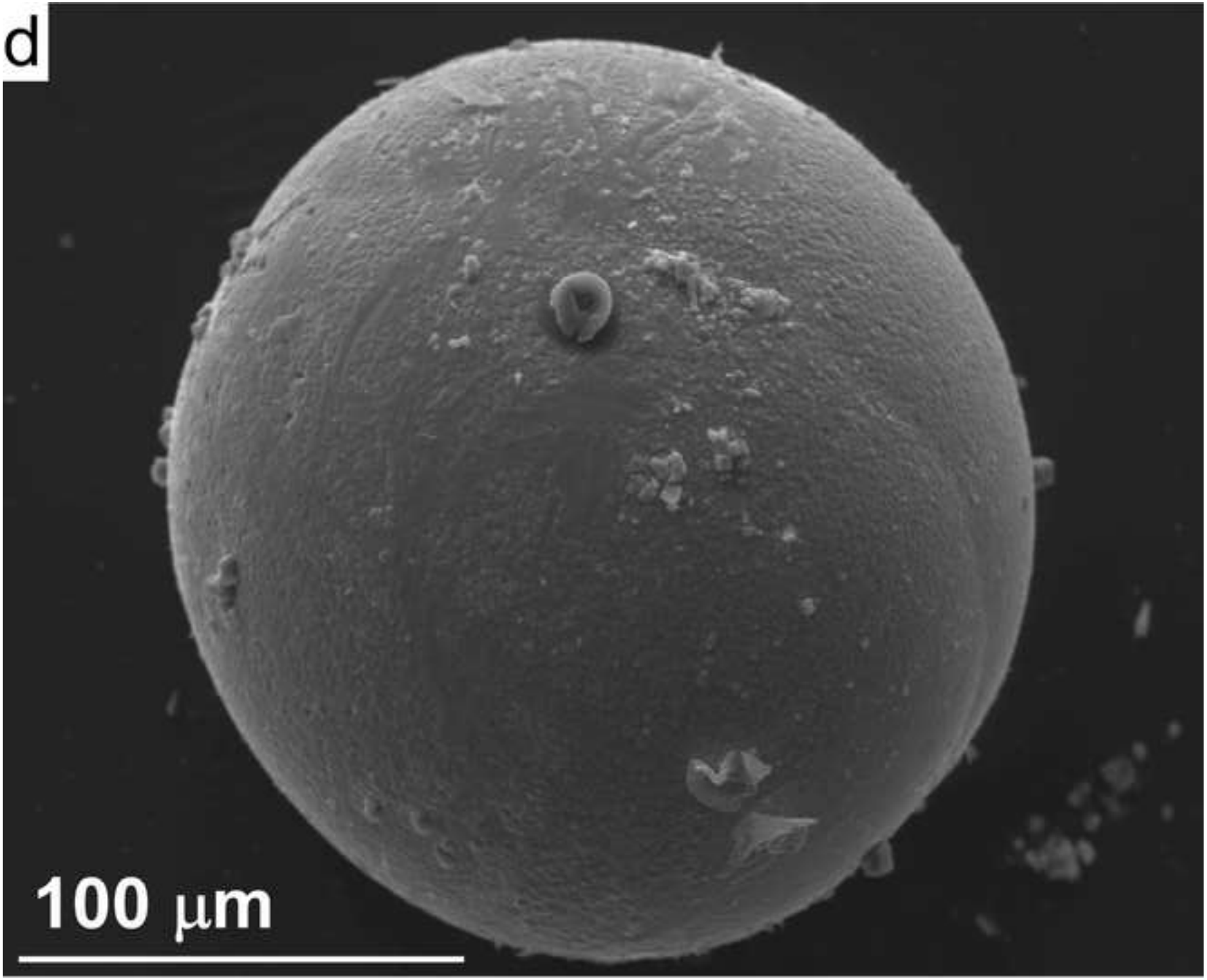

fig.4a
Click here to download high resolution image

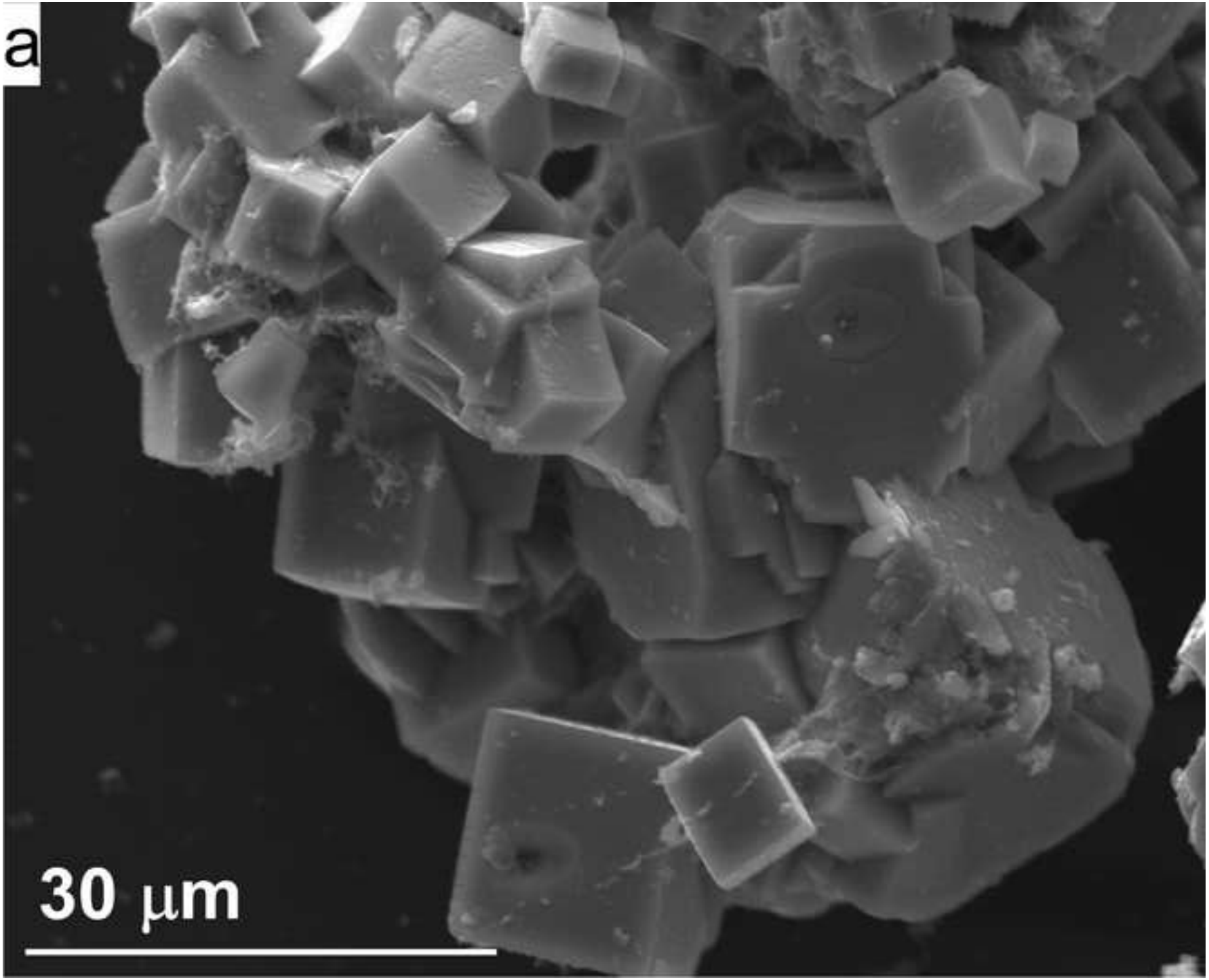

fig.4b

Click here to download high resolution image

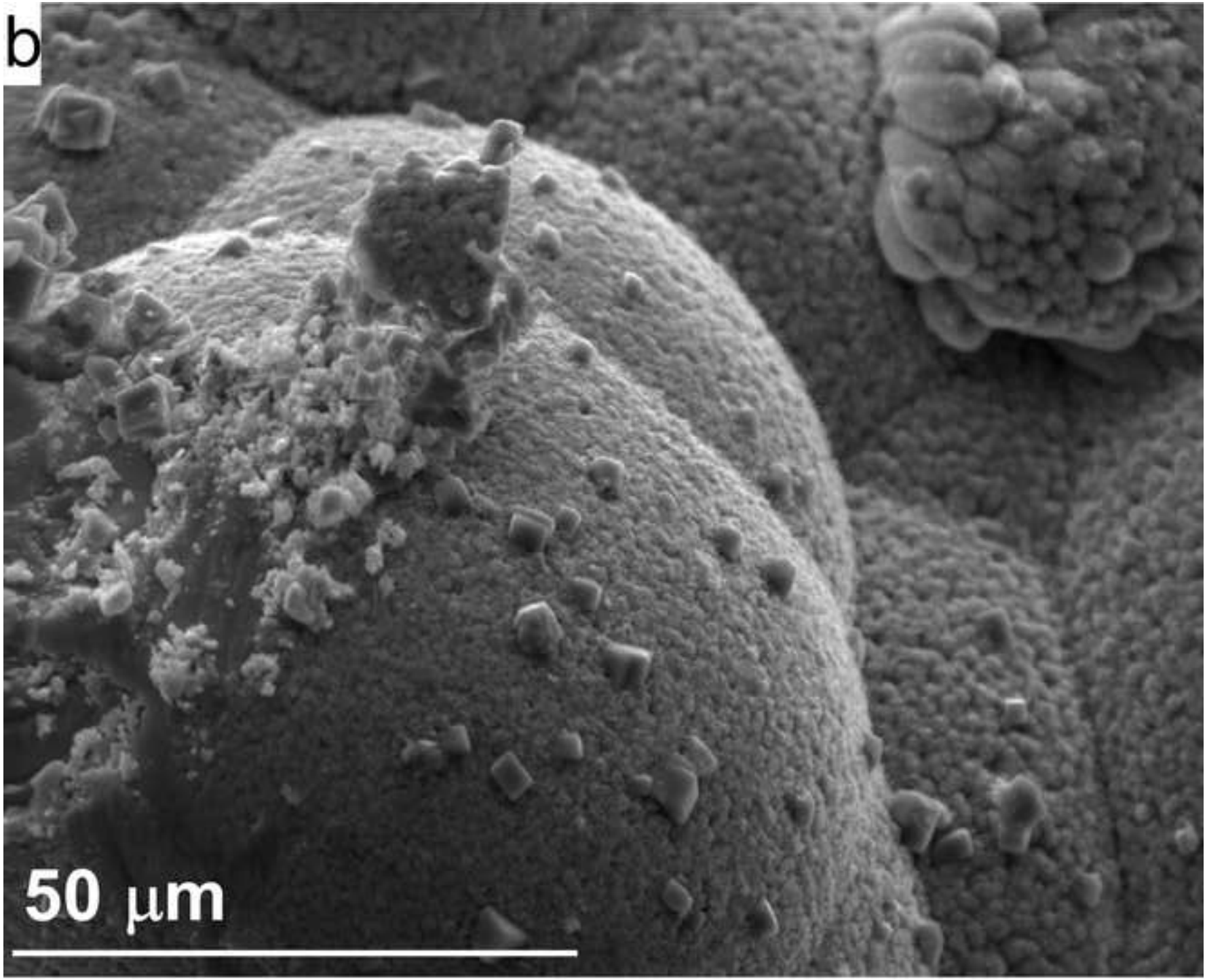

fig.4c
Click here to download high resolution image

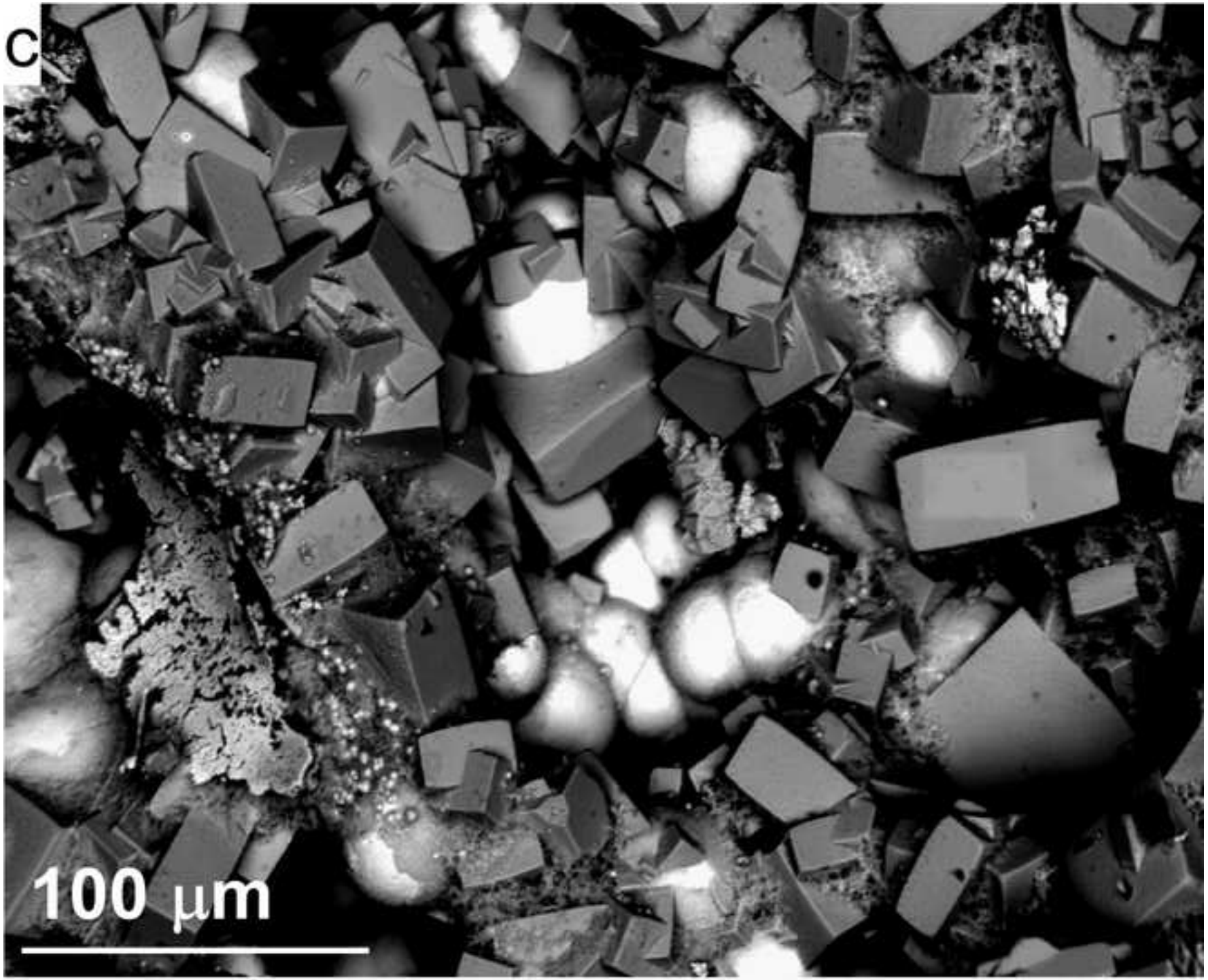

fig.4d
Click here to download high resolution image

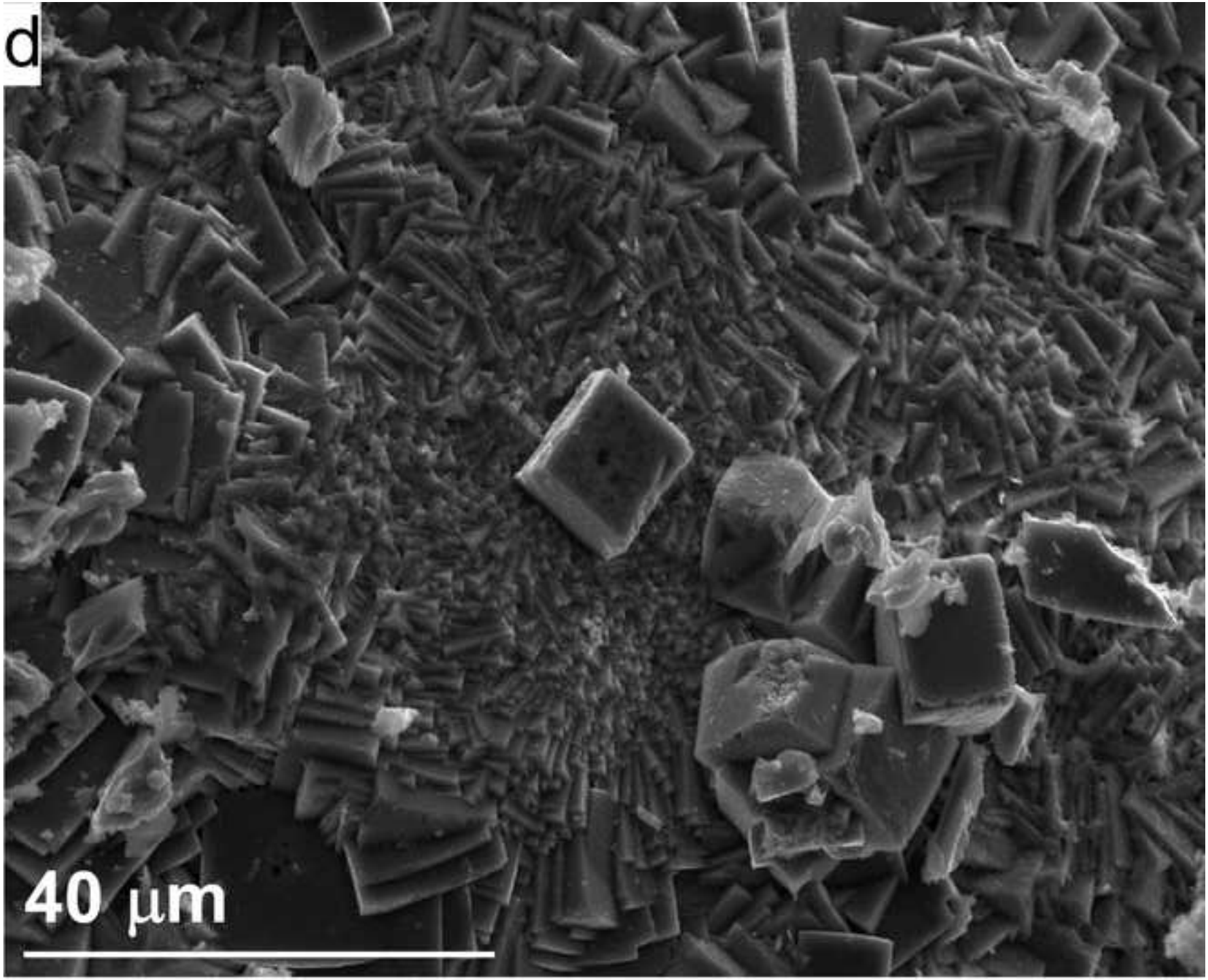

fig.5a
Click here to download high resolution image

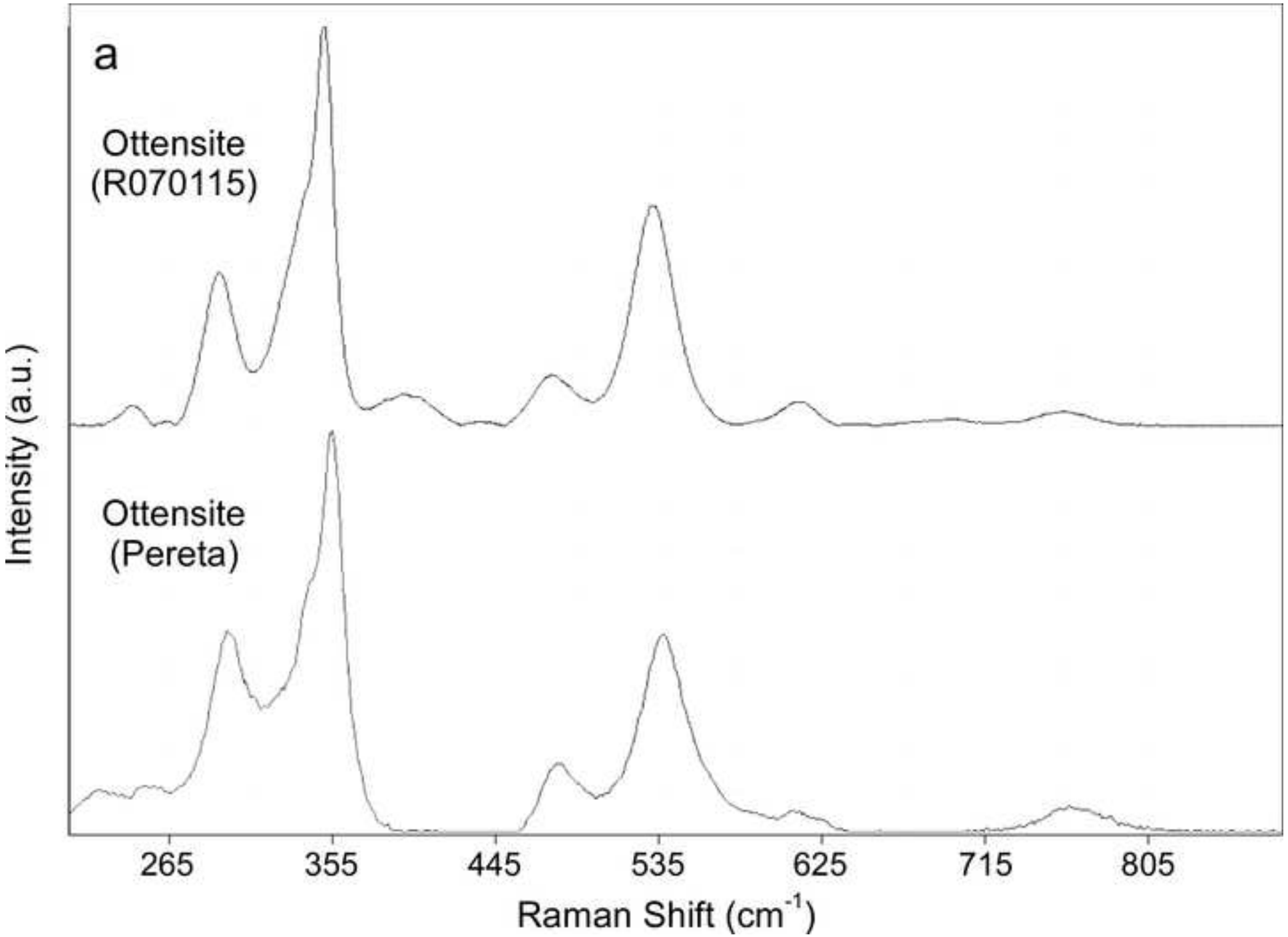

Table 6

Sb	– O(1) ×2	1.971(6)
	– O(2) ×2	1.987(7)
	– O(3) ×2	1.970(6)
<Sb−O>		1.976
Na	– O(1) ×2	2.420(7)
	– O(2) ×2	2.402(7)
	– O(3) ×2	2.391(6)
<Na−O>		2.404
	Sb—O(1)—Na	132.2(3)°
	Sb—O(2)—Na	132.3(3)°
	Sb—O(3)—Na	130.4(3)°

Table 6 Main interatomic distances (Å) and bond angles in the crystal structure of mopungite from Pereta mine

Fig. 5

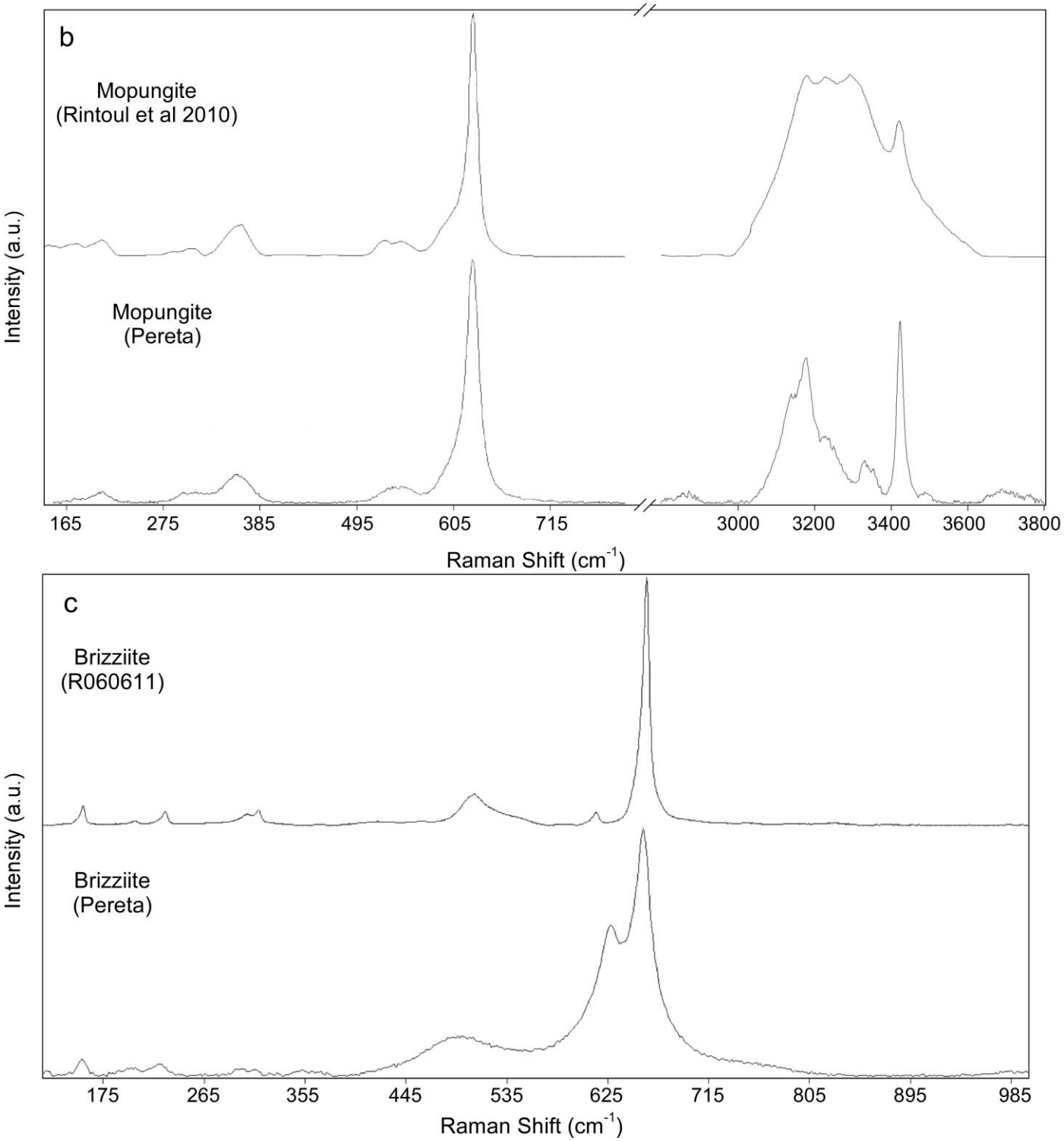
b
Mopungite
(Rintoul et al 2010)
Mopungite
(Pereta)
Intensity (a.u.)
165
275
385
495
605
715
3000
3200
3400
3600
3800
Raman Shift (cm-1)
c
Brizziite
(R060611)
Brizziite
(Pereta)
Intensity (a.u.)
175
265
355
445
535
625
715
805
895
985
Raman Shift (cm-1)

Fig.6

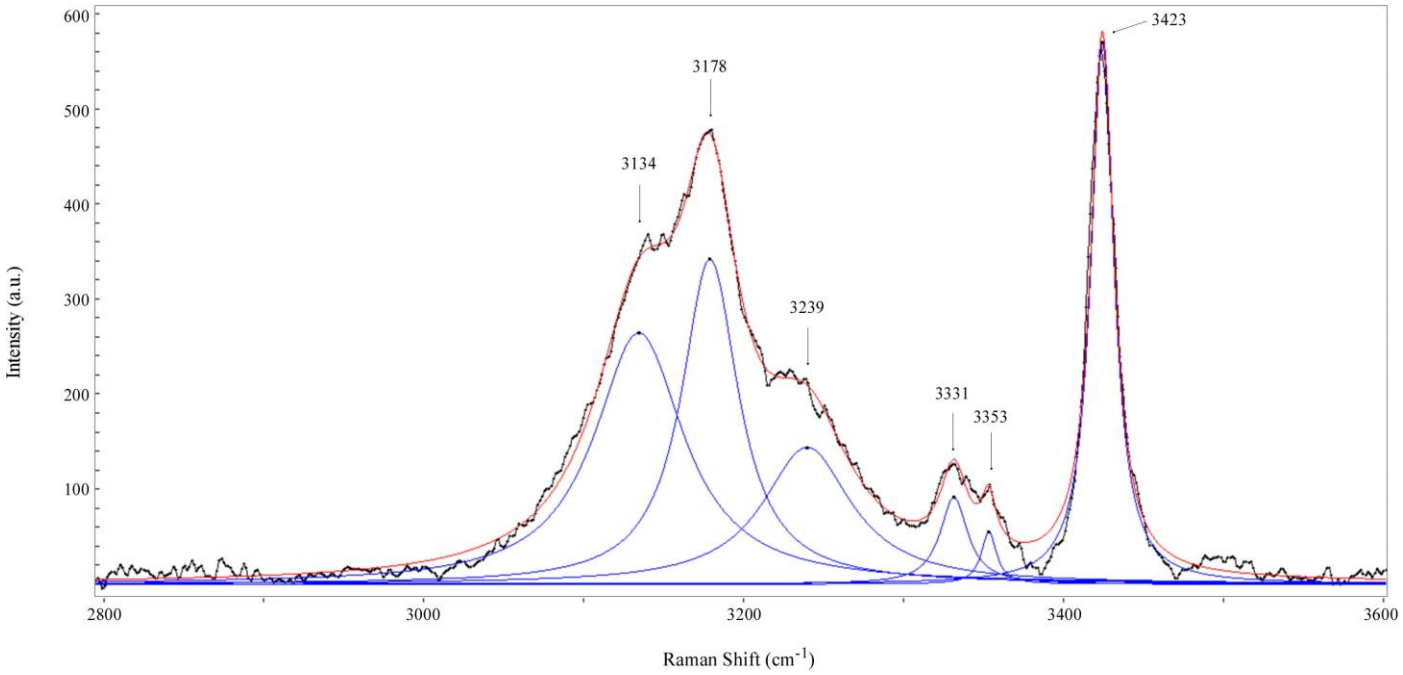
3423
3178
3134
3239
3331
3353
Intensity (a.u.)
Raman Shift (cm-1)
600
500
400
300
200
100
2800
3000
3200
3400
3600

fig.6

Click here to download high resolution image

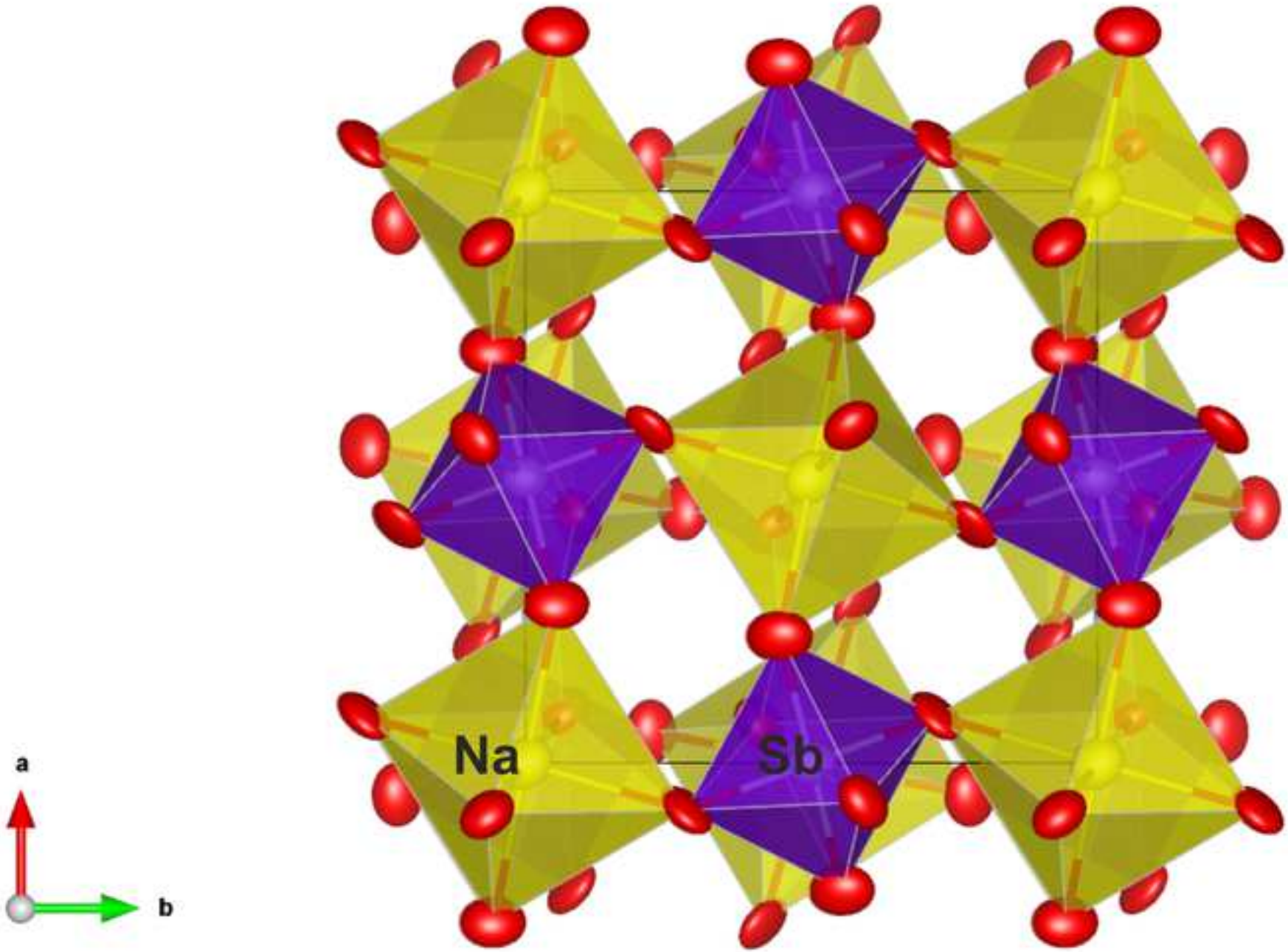

fig.7

Click here to download high resolution image